Biosensors and Bioelectronics 168 (2020) 112509

Contents lists available at ScienceDirect

Biosensors and Bioelectronics

journal homepage: http://www.elsevier.com/locate/bios

Laser scribed graphene: A novel platform for highly sensitive detection of electroactive biomolecules

Abdelghani Ghanam [a,1], Abdellatif Ait Lahcen [b,1], Tutku Beduk [b], Husam N. Alshareef [c], Aziz Amine [a,*], Khaled Nabil Salama [b,**]

[a] Chemical Analysis and Biosensors Group, Laboratory of Process Engineering and Environment, Faculty of Science and Techniques, Hassan II University of Casablanca, B.P 146, Mohammedia, Morocco

[b] Sensors Lab, Electrical Engineering Program, Advanced Membranes and Porous Materials Center (AMPMC), Computer, Electrical and Mathematical Science and Engineering Division, King Abdullah University of Science and Technology (KAUST), Thuwal 23955-6900, Kingdom of Saudi Arabia

[c] Materials Science and Engineering, Physical Science & Engineering Division, King Abdullah University of Science and Technology (KAUST), Thuwal, 23955-6900, Saudi Arabia

ARTICLE INFO

Keywords:
Laser-scribed graphene
Biosensor platform
Biomolecules
Phenolic compounds
Paracetamol

ABSTRACT

Laser-scribed graphene electrodes (LSGEs) have recently shown a potential for the development of electrochemical biosensors thanks to their electronic properties, porous structures, and large surface area that can support the charge transfer. In this paper, the authors present a comparative study of the electrochemical performances of LSGEs with the conventional screen-printed carbon electrodes (SPCEs) toward the detection of most commonly used phenolic compounds and biomolecules. Cyclic voltammetry measurements showed a significant enhancement in the electron transfer rate of all tested electroactive species at LSGEs compared to conventional SPCE. We have suggested, for the first time, a mechanistic study for catecholamine redox reactions at LSGE as the electron transfer–chemical reaction–electron transfer mechanism. Moreover, the excellent performances of LSGE were observed in terms of the electrocatalytic detection of paracetamol (PCM). Therefore, the second part of this study compared the analytical performances of LSGE and SPCE with respect to the detection of PCM. The LSGE allows a fast and reversible system for PCM with a low ΔE_p of 88 mV while the SPCE exhibits a quasi-reversible system with a higher ΔE_p of 384 mV. The LSGE demonstrated a PCM linear range of concentration between 0.1 μM and 10 μM, with a detection limit of 31 nM. In addition, the LSGE showed a successful applicability with good selectivity and sensitivity for PCM determination in real samples of pharmaceutical tablets. Hence, LSGEs could be an excellent platform for simple and low-cost electrochemical biosensor applications.

1. Introduction

Printing techniques (e.g., Inkjet, screen printing) for the elaboration of bare electrodes, as well as other printing techniques, are widely used for the development of sensing platforms in the field of electrochemical sensors and biosensors (Ahmad et al., 2018). Laser-scribed graphene (LSG) is an emerging electrode material that has received significant attention recently due to a variety of attractive features for sensing. For one, LSG is a three-dimensional (3D) graphene electrode, which can be printed using a mask-less process from precursor materials such as carbon, polymers, or biopolymers, thus enabling multiple ways to control the morphology, composition, and printing of the LSG (Kurra et al., 2019). In addition, by introducing gases during laser writing or inorganic and elemental species in the precursor polymer solution, the LSG electrode can be doped with various dopants (Chen et al., 2016; Hwang et al., 2015; Kurra et al., 2019; Lee et al., 2020; Zhang et al., 2018a). These features allow the fabrication of printed LSG electrodes with a variety of attractive characteristics including tunable 3D morphology, relatively high conductivity, high electrocatalytic activity, high electroactive surface area, dopant type and concentration, and defects (Griffiths et al., 2014; Kurra et al., 2019; Ye et al., 2018; You et al., 2019; Zhang et al., 2019a). The LSG based sensor platform can be

* Corresponding author.
** Corresponding author.
E-mail addresses: a.amine@univh2m.ac.ma (A. Amine), khaled.salama@kaust.edu.sa (K.N. Salama).
[1] Author Contributions: A.G. and A.A.L have contributed equally to this work

https://doi.org/10.1016/j.bios.2020.112509
Received 6 June 2020; Received in revised form 3 August 2020; Accepted 9 August 2020
Available online 19 August 2020

easily formed using a photothermal process, allowing patterning of the commercial flexible polyimide (PI) substrate and leading to the production of one-step porous graphene film (Lin et al., 2014; Beduk et al., 2020). Indeed, the photothermal process used to pattern the graphene film was based on CO_2 laser that converts the hybridized carbon sp^3 into carbon sp^2 as a result of the pulsed laser irradiation leading to the breaking of N–C, C–O, and C═O bonds. As a result, the aromatic compounds rearranged into a material structured in a graphene-manner (Cardoso et al., 2019). LSG based electrochemical (bio) sensors have found many successful applications in recent years for the detection of biomarkers, neurotransmitters and biomolecules (Fenzl et al., 2017; Nayak et al., 2016; Xu et al. 2018a, 2018b; Xuan et al., 2018).

The present study describes the electrochemical performance of LSG electrodes (LSGEs) in the determination of a wide range of commonly interesting phenolic compounds and biomolecules in comparison with the standard screen-printed carbon electrodes (SPCE) from DropSens Company.

Phenolic compounds are common constituents of variety of beverages, and are considered to be the major sources of antioxidants (Adebo and Medina-Meza, 2020; Talarico et al., 2015). Those compounds are composed of one or many hydroxyl group (-OH) attached to an aromatic group with benzene (de Moraes et al., 2019). A variety of phenolic groups exist in nature, including vitamins, hormones, amino acids, and antioxidants related to phenolic compounds (Vinson, 2019).A number of biological properties of phenolic compounds have been reported, including antibacterial, antitumor, anti-inflammatory, and antioxidant properties (Jesus et al., 2019; Nadifiyine et al., 2013). One of the most important biological properties of phenolic compounds is the antioxidant effect, which occurs as a result of the ability of phenolic groups with the ability to reduce the toxic effect of radical compounds and reactive oxygen species (Scalbert et al., 2005). Indeed, those compounds are able to reduce the risk of diseases-related to oxidative stress, including neurodegenerative disorders, cardiovascular diseases (Della Pelle et al., 2015). There are many important electroactive molecules are based on phenolic substances such as catechol, hydroquinone, caffeic acid, and paracetamol. The sensing of these molecules using enzymatic biosensors (mainly tyrosinase, laccase, and peroxidase sensors) has been widely reported in the literature (Attar et al., 2015; Nadifiyine et al., 2013; Palanisamy et al., 2017; Wee et al., 2019). Ascorbic acid is often presented as a strong interfering specie in the determination of such molecules (Tyszczuk-Rotko et al., 2014; Xu et al., 2019). For example, paracetamol (named also acetaminophen) and ascorbic acid are two molecules that are widely used as active compounds in several pharmaceutical drugs (Bayraktepe et al., 2019; Li et al., 2014; Zhang et al., 2018b). Thus, the development of highly sensitive and selective analytical tools for the detection of these compounds in pharmaceutical formulations as well as in body fluids is of great interest. Many interesting bioactive molecules such as neurotransmitters are also based on catechol groups. Those biomolecules provide a reversibility property by using cyclic voltammetry, leading to the oxidation of phenol to quinone and vice versa (Ramirez et al., 2016). Levodopa (L-Dopa), dopamine (DA), and epinephrine biomolecules are of great importance for human health. Those catecholamines and their precursors act as hormones and neurotransmitters in the mammalian physiological system. Therefore, the study of these biomolecules has boomed in the last decade in the field of electrochemical biosensors (Anithaa et al., 2017; Azzouz et al., 2019; Biswas et al., 2020; Ji et al., 2019; Xu et al., 2018a).

Many conventional analytical methods have been reported for the detection of phenolic compounds, such as high-performance liquid chromatography coupled mass spectrometry HPLC-MS (Tohma et al., 2017), electrophoresis (Lu et al., 2016), and UV-visible spectrophotometry (Viacava et al., 2018). However, these techniques are precise and accurate, but they require skilled personnel and a long time for analysis. Therefore, more practical and less demanding analytical strategies are highly necessary. Electrochemical sensors and biosensors have attracted attention due to their excellent analytical performances, instrumental portability, flexibility as well as their low-cost (Kumar et al., 2018; Lahcen and Amine, 2018; Zhang and Chen, 2019). As far as we know, this is the first report that presents a comparative study of the analytical performance between the LSGE and the SPCE towards the determination of versatile biological active molecules. This study could be very useful as a database on the use of LSGEs for the detection of these biomolecules. A mechanistic study was also suggested for the presented catecholamines at LSGEs and SPCEs. Herein, paracetamol PCM was selected as a target analyte due to its high electrocatalytic performance as well as the significant enhancement of the electron transfer rate at the LSGEs. The LSGE allows for the electrochemical behavior change of PCM from quasi-reversible electrochemical system, as at the SPCE to a fast and reversible system without any further modification of the electrode surface. In addition, the LSGE provides selective and sensitive PCM determination in the presence of ascorbic acid in pharmaceutical formulation samples. Thus, the LSG as sensing platform demonstrated excellent sensing features and could be a potential alternative to the commercially printed sensors for novel promising biosensor applications.

2. Materials and methods

2.1. Chemicals and reagents

The electroactive compounds, catechol (CC), hydroquinone (HQ), caffeic Acid (CA), paracetamol (PCM), ascorbic acid (AA), L-Cysteine (L-Cys), L-Dopa, and some catecholamines such as epinephrine (EP), or adrenaline (AD), and dopamine (DA), (Fig. 1S), were obtained from Sigma Aldrich and were used without further purification. 10 mM of stock solutions were prepared in deionized water and were stored at 4 °C. All supporting electrolyte solutions at fixed pH were prepared by using the analytical grade reagents dissolved in distilled water, H_3PO_4, Na_3PO_4, Na_2HPO_4, and KH_2PO_4 which were purchased from Solvachim, Morocco.

2.2. Apparatus and electroanalytical techniques

Cyclic voltammetry (CV), square-wave voltammetry (SWV), and amperometry measurements were carried out using an electrochemical instrument PalmSens (BV Houten, the Netherlands) connected to a computer and controlled by software named PSTrace 3.0. An electrochemical cell containing a three-electrode system was used. A glassy carbon electrode (GCE), a SPCE from DropSens Company, and a LSGE, with diameter of 3 mm, 4 mm, 3 mm respectively were used as working electrodes respectively. The reference electrode was a saturated calomel electrode (SCE) which is saturated with 3 M KCl, while a bare of stainless steel was used as a counter electrode.

The X-ray diffraction data were recorded using an X-ray diffractometer (XRD, Bruker Corporation, D8 ADVANCE, and Karlsruhe, Germany) with Cu Kα radiation (1.5406 Angstrom) and a 2θ range of 20–80. A LabRAM ARAMIS Raman spectrometer was used to obtain Raman spectra with a 473 nm cobalt laser source excitation at room temperature (Horiba Scientific). Electrode surface morphology was investigated by field emission scanning electron microscopy (FESEM; Carl Zeiss, Merlin).

2.3. Fabrication of the laser scribed graphene electrodes

The predesigned LSG three electrode system was prepared on a commercially available substrate PI sheet (Kapton Width: 12", Utech Products, USA). A CO_2 laser (Universal Laser Systems® PLS6.75) with a wavelength of 10.6 μm and a spot size of ~150 μm was used to irradiate a PI sheet to produce graphene electrodes as the photothermal process leads to molecular rearrangements (Fig. 1a). A polymer precursor was cleaned before the scribing process for the fabrication of three electrode sensing system (2.8 cm × 1.2 cm). To achieve the best graphene quality

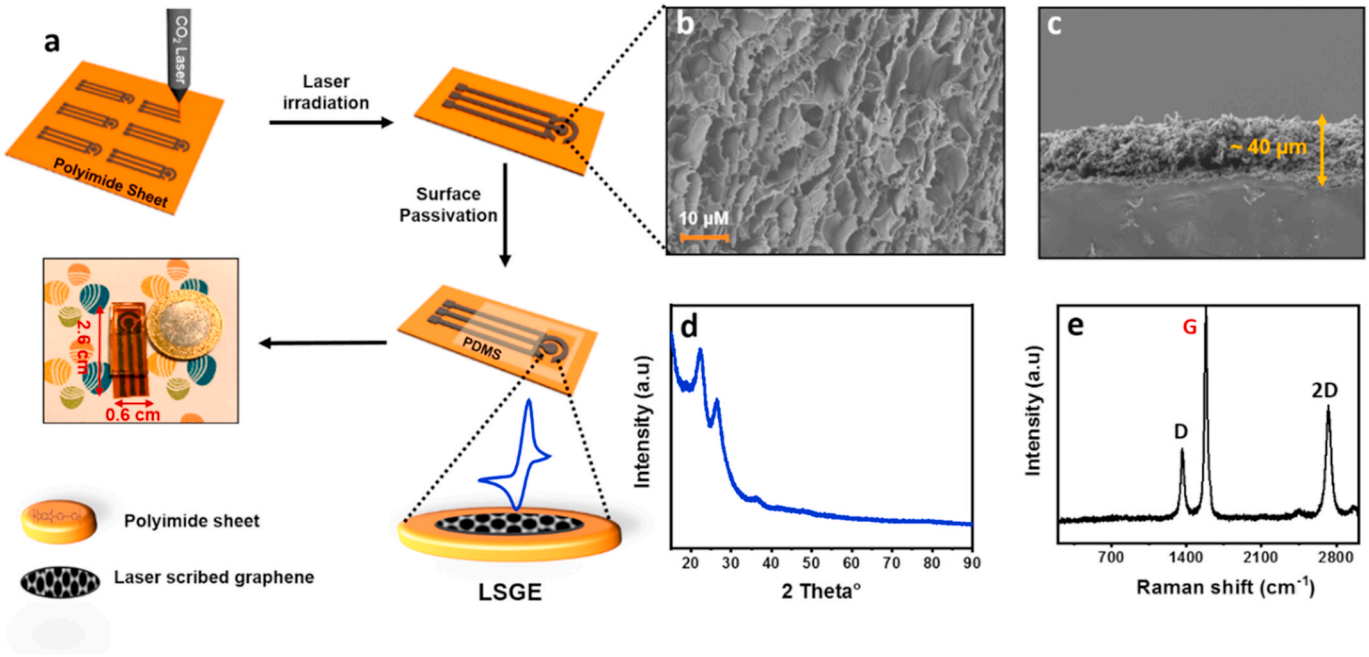

Fig. 1. (a) Schematic representation of the fabrication of LSG based on laser irradiation of the polyimide substrate; **b)** FESEM image of LSG; **(c)** Cross-section of LSG; **(d)** XRD spectrum of LSG; **(e)** Raman Spectrum of LSG.

formation, the laser scribing speed and power were optimized to fabricate the LSG electrodes while using an inert gas flow to minimize the heteroatom bonding effect. Laser power, speed, and z distance were recorded as 3.2 W, 2.8 cm/s and 2.5 mm, respectively, at 1000 pulses per inch to produce the best-quality multilayer graphene with high conductivity.

2.4. Detection of electroactive species

The potential was scanned with CV measurement at a well-defined potential window, depending on the electroactive compound studied, with 8 mV as the step potential and a scan rate of 50 mV s^{-1}. The most commonly used phenolic compounds and biomolecule electroactive species were selected to study the electrochemical behavior of LSGE in comparison with SPCE.

0.1 M PBS at pH 7.0 containing an appropriate amount of each one of these analyte was used as indicated in CV experiments and summarized in Table 1S.

SWV measurements were recorded by scanning the potential in the range +0.0 V to +0.6 V vs. SCE at the pulse amplitude, 25 mV with the frequency of 10 Hz and step potential of 8 mV on the SPCE, GCE, and LSGE to determine the limit of detection (LOD) of PCM. Amperometric measurements of hydrogen peroxide and L-Cysteine were carried out under a stirring solution (300 rpm) at the applied potential +1.00 and + 0.45 V, respectively, using both the SPCE and the LSGE in 0.1 M PBS (pH 7.0).

2.5. Preparation of real sample and selectivity test

Paracetamol is the main component of several drugs, either alone or in combination with other bioactive compounds, such as AA which is considered to be one of the molecules potentially interfering with PCM when measured electrochemically in real samples. To prepare the real sample, one tablet of the drug, Doliprane Vitamin C ®, labeled Paracetamol 500 mg and Vitamin C 150 mg per tablet, was crashed and dissolved into 100 mL of a solution of 0.1 M PBS (pH 7.0) under magnetic stirring and then stored at 4 °C. The final concentrations were 33.07 mM and 8.52 mM for PCM and AA, respectively. Doliprane Vitamine C ® was chosen because it contains AA, which oxidizes at a very similar potential to PCM.

3. Results and discussion

3.1. Characterization of the LSGE

The laser irradiation of the PI sheet using a photothermal process leads to the production of the LSG sensors. The CO_2 laser irradiation allows the rearrangement of the aromatic compounds of the PI into a graphene-like structures. After patterning the three electrodes system, a PDMS well is used to passivate and to define the sensor working area. As a result, the final LSG sensor dimensions were 0.6 cm/2.6 cm as shown in Fig. 1a.

Fig. 1b presents the FESEM image of the LSGE that exhibit a large number of graphene layers with high porosity. The cross-section of the LSG sensor is equivalent to around 40 µm thick approximately as shown in Fig. 1c.

The produced LSG sensing platform was characterized using XRD, Raman Spectroscopy and FESEM. The LSG crystallinity properties were investigated by XRD as shown in Fig. 1d. The results show two abundant peaks centered at $2\theta = 21.9°$ and 25.5°, indicating a (002) plane and the high degree of graphitization. The small peak around $2\theta = 36.5°$ belongs to (100) reflections that are associated with an in-plane structure (Lin et al., 2014).

Fig. 1e presents the characterization of the fabricated LSG using Raman spectroscopy.Three main peaks D (1359), G (1581), and 2D (2725), are present in the spectrum clearly confirming the graphene formation by LSG technology (Lin et al., 2014). The D and 2D bands could be attributed to the primary in-plane and second-order in-plane vibrations, respectively. As can be seen in the spectrum, the G peak is more intense compared to the D band. It should be noticed that previous studies reported a ratio value of I_{2D}/I_G attributed to the number of graphene layers (Ramlan et al., 2019). The ratio calculated in this study is around 0.73, correlating with the formation of graphene multilayers.

3.2. Electrochemical behavior of electroactive species

The electrochemical behavior of all tested phenols and substituted phenolic compounds, such as PCM, CA, catecholamines (EP, DA), and their precursor L-Dopa, L-Cys, AA, and hydrogen peroxide was recorded by CV at 50 mV s^{-1} at the SPCE and the LSGE in 0.1 M PBS, pH 7.0. Table 1S illustrates the summary of CV data for all tested molecules. Moreover, Fig. 2a and b shows the peak-to-peak separation ($\Delta E_p = E_{pa} - E_{pc}$) of the analytes tested, with the redox behavior being quasi-reversible or reversible on both the SPCE and the LSGE.

As indicated in Table 1S, Fig. 2a and 2b, the anodic peak potential of all tested molecules is shifted to the negative potential values, and there is a meaningful decrease in the ΔE_p for reversible molecules, indicating that the fast electron transfer occurred at the LSGE. This can be explained by the high porosity of the 3D LSGE working electrode as well as the graphene-like structure defects. These properties assure a fast electron mobility at the interface-electrolyte/LSG sensing area. Furthermore, among all tested molecules, PCM showed a significant enhancement of electron transfer at the LSGE and peak-to-peak separation, (ΔE_{LSGE}) was over 4-fold smaller in respect to the bare SPCE (ΔE_{SPCE}).

3.2.1. Electrochemical behavior of HQ, CC, PCM, and CA

The CVs in Fig. 2 depict the electrochemical behavior of the bare commercial SPCE and the LSGE in 0.1 M PBS (pH 7.0), towards HQ, CC, PCM, and CA. The SPCE exhibits a quasi-reversible redox behavior with a higher ΔE_p of 384, 340, 280, and 184 mV, respectively versus SCE, for all analytes. However, the LSGE showed a significant enhancement in the electrochemical performances, and its ability to change the redox behavior of all analytes in respect to the conventional SPCE. The electron transfer process at the LSGE is significantly improved and becomes faster with a lower ΔE_p of 88, 80, 80, and 56 mV versus SCE for PCM, HQ, CC, and CA, respectively. To get more information about the electroanalytical performances of LSGE sensors, a second successive voltammetric scan was performed to evaluate the electrochemical fouling and stability of the electrodes. Electrode fouling is considered the main challenge preventing the phenolic compounds form being analyzed quantitatively in the electroanalysis field. It affects the reusability of the developed sensors, because the non-conductive polymeric film adsorbed due to their oxidation products subsequently causes a remarkable decrease in the electrochemical signal after each successive scan of such electrochemical technique (Ghanam et al., 2017; Talarico et al., 2015). Indeed, a slight decrease of the peak current intensity between two successive scans was observed for PCM at the SPCE. However, this was not observed at the LSGE, while similar results, within experimental error, were obtained on both electrodes for HQ, CC, and CA.

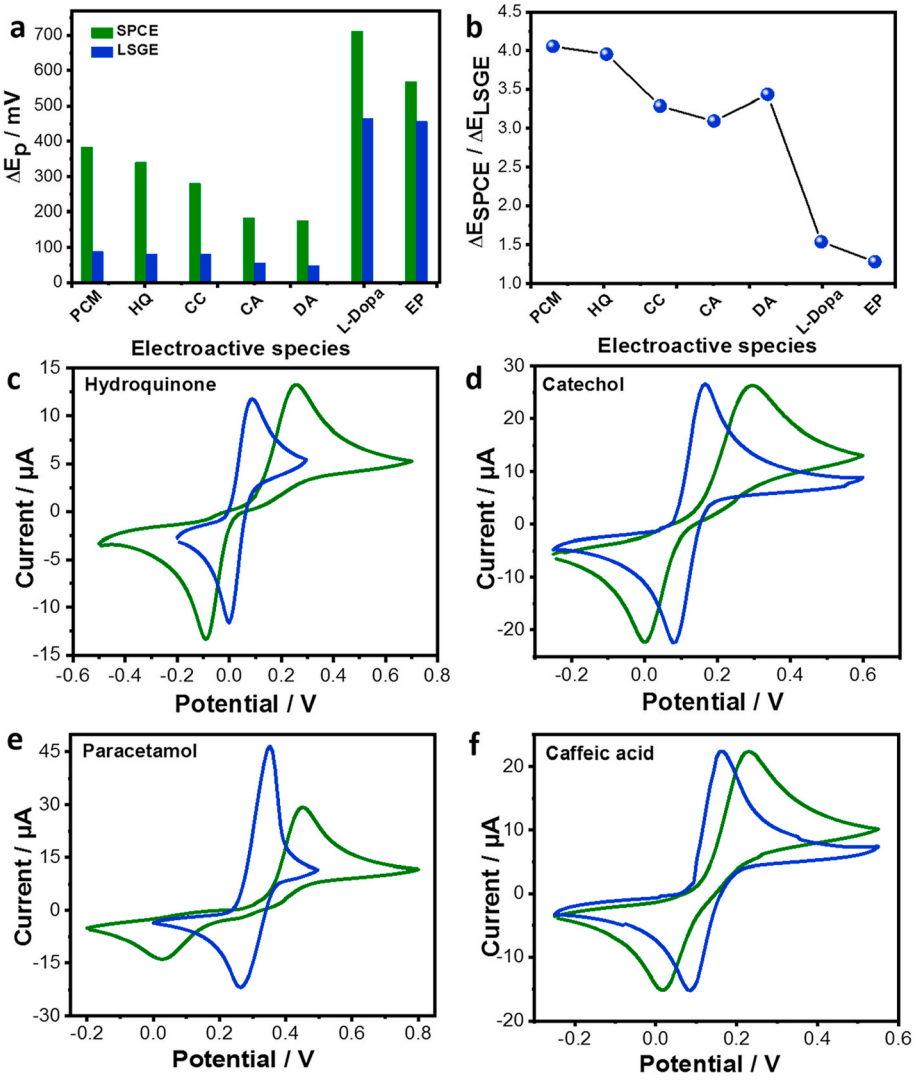

Fig. 2. (a) Peak-to-peak separation (ΔEp) on SPCE (**green**) and LSGE (**blue**) and **(b)** change in the $\Delta E_{SPCE}/\Delta E_{LSGE}$ ratio of quasi-reversible and reversible electrochemical system obtained by CV at a scan rate of 50 mV s^{-1} in 0.1 M PBS, pH7.0. CVs at bare SPCE (**green line**) and LSGE (**blue line**), scan rate 50 mV s^{-1} in 0.1 M PBS, pH 7.0 in presence of **c)** hydroquinone 0.5 mM, **(d)** catechol 1 mM, **(e)** paracetamol, and **(f)** caffeic acid. (For interpretation of the references to colour in this figure legend, the reader is referred to the Web version of this article.)

3.2.2. Electrochemical behavior of catecholamines and their precursor L-Dopa

3.2.2.1. A proposed mechanistic study. The electrochemical behavior of certain catecholamines, 0.5 mM DA, 1 mM EP and their precursor 1 mM L-Dopa, were also investigated using CV in 0.1 M PBS, pH 7.0. As can be seen in the CVs of DA (Fig. 3ai), one oxidation peak (**O_1**) in the direct scan and one reduction peak (**R_1**) on the reverse scan were observed at both the SPCE and the LSGE. A quasi-reversible redox process at the SPCE with a ΔE_p of 176 mV and reversible peaks with a fast electron transfer at the LSGE with a lower ΔE_p of 48 mV were obtained. Moreover, the remarkable reversibility in CV is ascribed to the electro-oxidation of DA to open-chain quinone by a simple deprotonation process. This can be explained according to a recently reported study on the DA oxidation pathway (Schindler, 2019). This study showed that the reaction mechanism of DA oxidation is strongly depending on the pH, so a slight change can significantly alter the species distribution, pathway, and kinetics of the electrochemical reactions due to the high reactivity of DA. In addition, even at pH 7.0, the amine groups still in solution as ammonium ions (-NH^+_4) are the predominant species. Therefore, the implication of Michael addition and Schiff-type reactions with cyclization to indole ring-containing products can only occur with a lower reaction rate (i.e., slow cyclization rate) as well as at pH values higher than 8.0 (Schindler and Bechtold, 2019). Hence, in our case (0.1 M PBS, pH 7.0) limited for only the open-chain o-quinones of the dopamine (**R_1**) to dopamine-quinone (**O_1**) in Fig. 3 aii.

The oxidation-reduction reactions of EP and L-Dopa showed excellent and similar behavior with a large potential window between the oxidation and the reduction peaks of 712 mV and 464 mV versus SCE (L-Dopa); 568 and 456 mV versus SCE (EP), at the both the SPCE and LSGE, respectively. However, the LSGE showed excellent performance toward EP and L-Dopa electrocatalytic reactions as well as detecting their oxidation products successfully.

As shown in Fig. 3 bi and Fig. 3 bii for EP and L-Dopa, only one oxidation peak (**O_1**) was found at the first anodic scan at the SPCE at +316 mV and at +172 mV at the LSGE for L-Dopa in the range from −0.5 to + 0.6V (Fig. S2a), compared to the results for EP at +288 mV at the SPCE and at +144 mV at the LSGE in the range −0.6 to +0.7 V (Fig. S2b). This behavior is due to the electro-oxidation of **R_1**-catecholamine to **O_1**-o-quinone as indicated in Fig. 3 biii. On the reverse scan (cathodic scan), for both L-Dopa and EP, the **O_1**-o-quinone to **R_1**-catecholamine did not occur. However, the o-quinone (**O_1**), once formed, cyclizes to aminochrome (**O_2**) via series of chemical reactions (1, 4 [Michael],addition) as indicated in Fig. 3 biii. Aminochrome (**O_2**) is electrochemically active and can be reduced to leucoaminochrome at the LSGE, leading to a reduction peak **R_2** (Fig. 3 bi and Fig. 3 bii), at −292 mV and −312 mV for L-Dopa and EP, respectively. Moreover, the cathodic peak potential at the SPCE was obtained at −396 mV and at

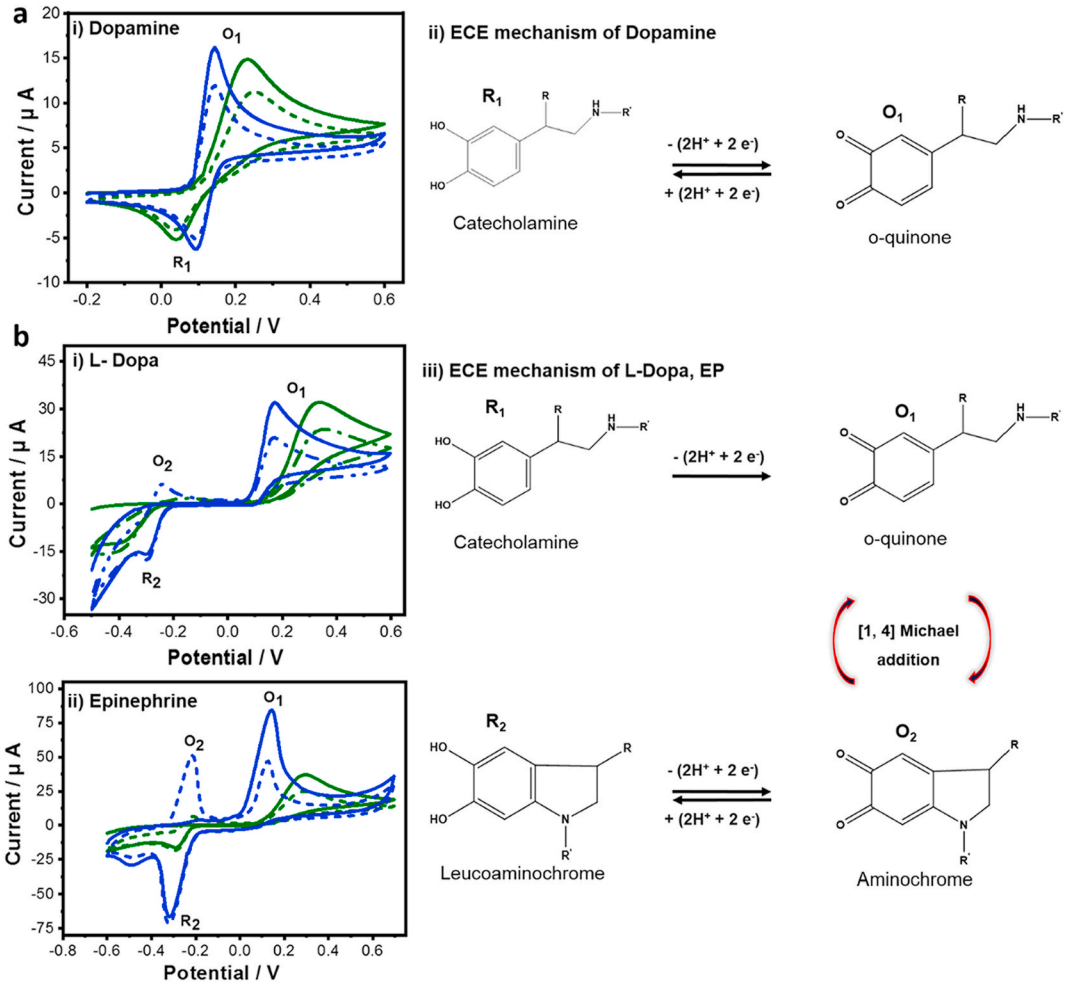

Fig. 3. CV responses of two successive scans at SPCE (**green line first scan** and **dotted line second scan**) and LSGE (**blue line first scan** and **dotted line second scan**), scan rate 50 mV s^{-1} in 0.1 M PBS, pH 7.0, in the presence of: **(ai)** 0.5 mM DA, **(bi)** 1 mM L-Dopa, and **(bii)** 1 mM EP. **(aii)** and **(biii)**The proposed mechanism the ECE mechanism for the oxidation-reduction reaction of catecholamines and their precursor L-Dopa. For all biomolecules, **R** and **R′** are, respectively, as follows: Dopamine,(H, H); L-dopa, (H, –COOH group); epinephrine, (OH, CH_3). (For interpretation of the references to colour in this figure legend, the reader is referred to the Web version of this article.)

−280 mV for L-Dopa and EP, respectively. Another oxidation peak (**O_2**) was observed in the successive second anodic scan (Fig. 3 bi and Fig. 3 bii) and more defined in Fig. 2Sc and Fig. 2Sd, which is clear at the LSGE at −244 mV for L-Dopa and −216 mV for EP and very small at the SPCE at −148 mV and at −216 mV of L-Dopa and EP, respectively. In addition, we observed that the anodic current intensities of the EP and L-Dopa decreased, as much as the current intensity of these peaks increased, as illustrated in Fig. 3 bi and Fig. 3 bii. Therefore, these peaks are generated by the irreversible oxidation of the catecholamines that is probably consumed after each scan. Indeed, the electrochemical behavior of EP and L-Dopa catecholamines, obviously remarked on LSGE encouraged us to study their oxidation-reduction reactions mechanism. Fig. 3 aii and Fig. 3 biii shows the proposed mechanism of the oxidation-reduction of catecholamines such as DA, EP, and L-Dopa, where the results can be explained according to the literature. Although the mechanisms of the electrochemical oxidation of EP have been previously discussed and verified (Hawley, 1967) (Schindler and Bechtold, 2019), it remains unclear whether the nature of mechanism is electron transfer-chemical reaction-chemical reaction (ECC) or electron transfer-chemical reaction-electron transfer (ECE). Indeed, our results tend to confirm the ECE mechanism, which is in agreement with the results reported by Wierzbicka and Sulka, 2016 (Wierzbicka and Sulka, 2016).

By the electrochemical oxidation of DA, EP, and L-Dopa presented different electrochemical behavior. The electrochemical oxidation of several catecholamines, such as DA, EP, and noradrenaline and their cyclization rate as a function of pH have been reported previously (Hawley, 1967). Indeed as mentioned above for DA, the pH has a significant effect on the mechanism pathway of EP and L-Dopa. At a low pH, an open-chain adrenalinequinone is protonated largely (pKa = 8.88). Therefore, the cyclization reaction is excluded, whereas adrenalinequinone (**O_1**) and L-Dopaquinone (**O_1**) produced by the electrochemical oxidation of AD and L-Dopa, **O_1/R_1**, (Fig. 3 biii), are probably unstable at pH 7.0, and subsequently transform quickly into aminochrome via the 1,4 [Michael] addition reaction and prevented the peak **R_1** from appearing in CV during the reverse scan (Hawley, 1967; Sanghavi et al., 2013). In addition, the quasi-reversible systems appeared obviously on the LSGE during the second scan for both EP and L-Dopa and could be probably attributed to the third electrochemical reaction (**O_2/R_2**) in Fig. 3 biii corresponding to the **O_2**-aminochrome –**R_2**-Leucoaminochrome equilibrium.

Thanks to their excellent electrocatalytic activity, LSGEs are considered to be promising sensors for detecting such generated compounds. Therefore, these sensors can be useful for the real-time detection of catecholamines in pharmacological samples as well as in biological microenvironments.

3.2.3. Electrochemical behavior of L-Cys, AA, and H_2O_2

The electrochemical behavior of totally irreversible molecules such as L-Cys, H_2O_2, and AA was evaluated at the SPCE and the LSGE. It can be seen clearly from Fig. 3S that the oxidation peak shifted to the negative potential values for all tested molecules at LSGE, which can be attributed to the electrocatalytic effect and the excellent conductivity of the LSGE compared to the SPCE. The results showed a high peak separation between the SPCE and the LSGE, $\Delta E_{SPCE\text{-}LSGE}$, 220, 230, and 296 mV of L-Cys, H_2O_2, AA, respectively. The obtained results are promising for amperometric measurements. In addition, approaching negative potentials, increases the signal-to-noise ratio and lowers the detection limit.

Thanks to the high sensitivity of amperometry (Amine, 2019), measurements were performed under magnetic stirring (300 rpm) in 0.1 M PBS, pH 7.0 at fixed potential using the SPCE and the LSGE on two examples of these molecules. Since the amperometric measurement of AA was already reported at the LSGE sensor, L-Cys and H_2O_2 were selected in order to calculate their LOD and show the advantages of the LSGE in amperometric detection compared to the SPCE (Nayak et al., 2016).

Fig. 4S shows the amperogram and calibration curve recorded at the SPCE the LSGE for L-Cys detection. Indeed, Table 2S summarizes the analytical features found for the SPCE and the LSGE in 0.1 PBS, pH 7.0. The detection limit of L-Cys at the applied potential of + 0.45 V was calculated to be 0.24 μM on the LSGE and 0.4 μM on the SPCE, while for H_2O_2, the limit of detections were obtained at +1.0 V versus SCE to be 2.00 and 5.00 μM on LSGE and SPCE, respectively.

3.3. Electrochemical study of paracetamol

Fig. 4a presents the CVs of PCM at the LSGE, SPCE and GCE. As indicated in Fig. 4a and Table 1S, the electrochemical behavior of PCM showed significant improvement in the electron transfer rate. These excellent electrocatalytic properties of LSGE are due to its porous structure with graphene defects which are not present in conventional SPCE. Moreover, the electrochemical behavior of PCM as quasi-reversible on bare electrodes has already reported on a GCE, SPCE, and Boron Doped Diamond Electrode (BDDE); (Ibanez-Redin et al., 2018) (Tyszczuk-Rotko et al., 2019; Zhang et al., 2019c). On the GCE and SPCE, PCM shows an irreversible redox behavior with small redox peaks. It is required to modify the working electrodes in order to change their redox behavior using several modifying agents, such as, PEDOT: PSS film (Wong et al., 2018). By contrast, on the LSGE, the anodic and cathodic peak currents increased significantly, and good reversibility was achieved with a fast electron-transfer system. Good reversibility was also achieved without engaging in the complicated process of further modifying of the electrode surface. In addition, the LSGE transformed PCM behavior from a fully quasi-reversible system (SPCE, GCE) with high ΔE_p (384 mV at SPCE and 440 mV at GCE) to a fast reversible system with lower peak separations of 88 mV. The electrochemical investigation of PCM was then selected for the rest of the work.

3.4. Effect of scan rate and pH on PCM measurement

To understand the mechanism of mass transport and electron transfer, it is necessary to consider the effect of scan rate, which is an important selection parameter. Fig. 4c shows CVs recorded at a different scan rate from 10 to 200 mV s^{-1} in 0.1 M PBS, pH 7.0 containing 100 μM of PCM. The plot log (Ip_a) versus the log (scan rate) obtained at the LSGE (Fig. 4d) showed good linearity, with the following linear regression equation:

$$\log (Ip_a) = 1.103 \times \log (v) - 0.753 \quad (1)$$

The slope obtained is almost one unity, indicating that the electro-oxidation of PCM at the LSGE was completely adsorption-controlled process. Therefore, the current might be proportional to the scan rate according to equation (2) (Sharp et al., 1979):

$$\log(Ip) = \log(v) + \log(\frac{n^2F^2A\Gamma}{4RT}) \quad (2)$$

where Γ represents the surface coverage concentration (mol.cm^{-2}), v is the scan rate (mv.s^{-1}), A (cm^2) is the electroactive surface area and Ip is the peak current. The electroactive surface area of the LSGE was calculated to be 0.168 cm^2 according to our previous work (Beduk et al., 2020). The number of transferred electrons has been calculated to be 2.09 using equation (3):

$$\Delta Ep = Ep - Ep_{1/2} \approx \frac{2.3RT}{nF} = \frac{59}{n} mV\ (25^\circ C) \quad (3)$$

The obtained surface coverage concentration of the LSGE is $\Gamma = 3.75 \times 10^{-7}$ mol cm^{-2}.

The effect of pH on the electrochemical signal was investigated in the pH range 3–11 at LSGE in the presence of 500 μM PCM in 0.1 M PBS. Fig. 4b shows the CVs obtained at different values of pH where the PCM are slightly dependent on the pH media, as indicated in Table 3S. The

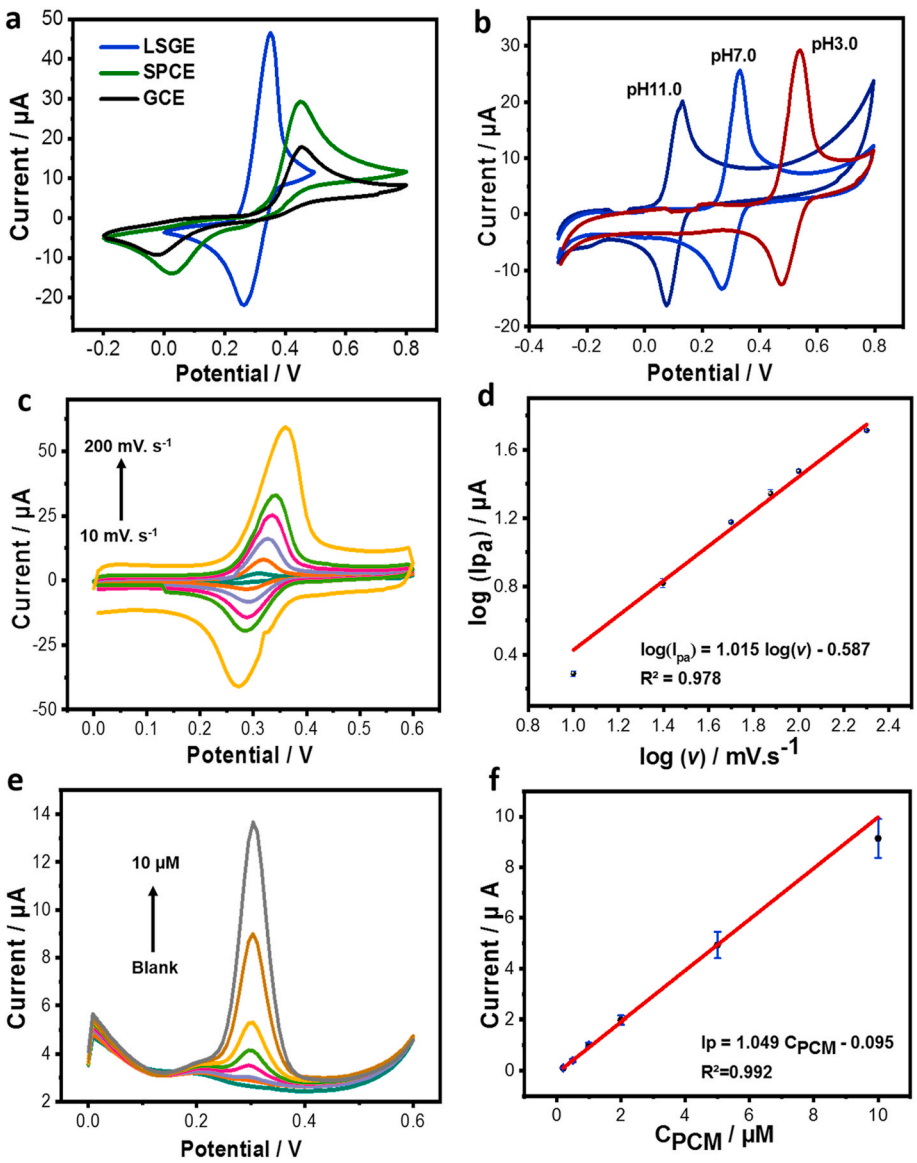

Fig. 4. (a) CV responses at the LSGE, the SPCE, and the GCE of 1 mM PCM in 0.1 M PBS, pH 7.0 at a scan rate of 50 mV s^{-1}.**(b)** CVs at different pH (3, 7, and 11) in 0.1 M PBS in the presence of 0.5 mM PCM at the LSGE. **(c)** CV responses obtained at the LSGE sensor for different scan rates (10, 25, 50, 75, 100, and 200 mV s^{-1}) in 0.1M PBS, pH 7.0 containing 0.1 mM PCM. **(d)** Linear plot of PCM oxidation peak log (Ipa) vs. log of scan rate. **(e)** SWV responses obtained at the LSGE for the successive addition of PCM (0.1–10 µM) in 0.1 M PBS, pH7.0. SWV conditions: E_{amp} 25 mV, E_{step} 8 mV, f 10 Hz. **(f)** Corresponding calibration plot.

majority of phenolic compounds tend to reach the highest electro-oxidation in a netrual pH medium. Hence, pH 7.0 was selected for the further experiments. The peak potentials showed a linear relationship against the pH, with regression equations for both electrochemical reactions $E_{p,a} = -0.051 \times pH + 0.692$, $R^2 = 0.999$ and $E_{pc} = -0.05 \times pH + 0.623$, $R^2 = 0.998$. In addition, from the Nernst equation, that is, $dEp/dpH = 2.303\ mRT/nF$ (m: number of protons H^+ and n : number of electrons), we can easily determine the ratio (m/n) from both the cathodic and the anodic slopes. From E = f (pH) curve, the ratios (m/n) were calculated to be 0.86 (oxidation) and 0.84 (reduction) which are almost one unit indicating that the number of protons (H^+) and electrons is equal.

3.5. Electroanalytical performances of the LSGE

3.5.1. Sensitivity of the LSGE to PCM detection

Under optimal conditions, SWV is known as a highly sensitive electroanalysis technique and is preferably used for a reversible redox system. This technique was used to evaluate the analytical performance of the LSG sensor in detecting PCM in 0.1 M PBS, pH 7.0. The SWV measurements were recorded in the PCM concentration range 0.1–10 µM. The results obtained from SWV (Fig. 4e), reveal a linear increase in peak currents with an increase in PCM concentration. The calibration curve in Fig. 4f presents the calibration curve in the range of 0.1–10 µM. The calculated linear regression equation was $Ip = 1.049\ C_{PCM} - 0.095$; $R^2 = 0.992$, and the sensitivity and LOD were calculated to be 1.049 ± 0.176 µA μM^{-1} and 31 nM, respectively. Table 1 summarizes the characteristics and analytical performances of the LSGE toward PCM detection compared to other reports in the literature. The table clearly shows that the LSGE allows the detection of a low PCM concentration without any of the further sensor modifications that usually require complicated and time-consuming steps. The ease of preparation of the LSGE in mask-free, mass production, as well as the fast response with high sensitivity due to the edge sites and defects on the graphene sheets, made it excellent sensor for the selective and sensitive detection of PCM.

3.5.2. Real sample analysis and selectivity test

Ascorbic acid is considered to be the agent that interferes most with biomolecules since it oxidizes at a potential value close to that of PCM and generally presents in combination with several drugs. Fig. 5 presents the detection of PCM using SWV in a real sample of pharmaceutical tablets of Doliprane Vitamin C ®, labeled Paracetamol 500 mg and Vitamin C 150 mg per tablet, dissolved in 0.1 M PBS, pH7.0. The PCM determination was then tested on the three electrodes in order to

Table 1
Summary of the analytical features of the developed electrochemical sensors for PCM detection.

Sensor configuration	Technique	Concentration range (μM)	LOD (μM)	Real sample	Reference
Modified electrodes					
SPCE/CB – ERGO	SWV	10–200	1.500	–	Ibanez-Redin et al. (2018)
MWCNT/ZnO–Au/GCE	SWV	0.05–20	0.009	Pharmaceutical formulation	Kenarkob and Pourghobadi (2019)
fMWCNT – CoPc/AuNPs/ GCE	SWV	1.49–47.6	0.135	Pharmaceutical formulation	de Holanda et al. (2016)
AgNPs-CB PEDOT:PSS/GCE	SWV	0.62–7.1	0.012	Synthetic urine and river water sample	Wong et al. (2018)
GAIN/CuE	DPV	1–700	0.012	Human urine	Taleb et al. (2018)
PEDOT/AG/GCE	AD	0.15–5880	0.041	Pharmaceutical formulation	
Pd/GO/GCE	DPV	0.005–0.5/ 0.5–80	0.002	Pharmaceutical formulation and human urine	Li et al. (2014)
PCA@Zn/Ni-ZIF-8-800/ GCE	DPV	0.08–1000	0.029	Pharmaceutical formulation and human urine	Zhang et al. (2019b)
Arg-G/GCE	DPV	0.5–100	0.05	Pharmaceutical formulation and serum sample	Zhang et al. (2018b)
ERG/GCE	AD/DPV	0.005–4/5–800	0.002/ 1.2	Pharmaceutical formulation and human serum	Adhikari et al. (2015)
SEP/MWCNTs/pPGE	DPV	0.059–60	0.018	Pharmaceutical formulation	Bayraktepe and Yazan (2020)
BiO-SPCEs	DPV	0.5–97	0.03	Pharmaceutical formulation, serum, urine, and saliva	Mahmoud et al. (2017)
AuNPs@TC8A/GN/GCE	DPV	0.5–120	0.1	Pharmaceutical formulation and human serum	Liu et al. (2019)
MIPs modified electrodes					
MIP/pABSA/GCE	DPV	0.05–100	0.043	Pharmaceutical formulation and human urine	Teng et al. (2015)
MIP/PB/GCE	DPV	0.001–100	0.0005	Pharmaceutical formulation and human urine	Dai et al. (2016)
MMIP/MCPE	DPV	0.06–50/50–200	0.017	Pharmaceutical formulation, human serum, and urine	Su et al. (2020)
Unmodified electrodes					
BDDE	DPV	0.065–32	0.430	Artificial urine sample	Niedzialkowski et al. (2019)
B:CNWE	DPV	0.032–32	0.281	Artificial urine sample	Niedzialkowski et al. (2019)
BDDE	DPV	0.1–200	0.013	Pharmaceutical formulation, blood, and serum samples	Karikalan et al. (2016)
BSPCE	DPV	0.05–190	0.013	Pharmaceutical formulation	Karikalan et al. (2016)
CPE	LSV	12.41–200	3.700	Synthetic urine sample	Guzman-Hernandez et al. (2016)
GCE	DPV	4–100	0.369	Pharmaceutical formulation	Engin et al. (2015)
LSGE	*SWV*	*0.1–10*	*0.031*	*Pharmaceutical formulation*	***Present work***

SPCE/CB-ERGO: Electrochemically reduced graphene oxide modified screen printed carbon electrode; MWCNT/ZnO–Au/GCE : Multi-walled carbon nanotubes/ZnO/ AuNPs modified glassy carbon electrode; **fMWCNT/CoPc/AuNPs/GCE**: AuNPs, functionalized multi-walled carbon nanotubes and cobalt (II) phthalocyanine modified glassy carbon electrode; **AgNPs-CB-PEDOT:PSS/GCE**: Silver NPs, carbon black, and poly(styrenesulfonate) modified glassy carbon electrode; **MWCNT-βCD/GCE**: Multi-walled carbon nanotube and β-cyclodextrin modified glassy carbon electrode; **GAIN/CuE**: graphene augmented inorganic nanofibers modified copper electrode; **PEDOT/AG/GCE**: PEDOT doped with Au@graphene core-shell NPs modified glassy carbon electrode; **Pd/GO/GCE**: Pd NPs on graphene oxide modified glassy carbon electrode; PCA@Zn/Ni-ZIF-8-800/GCE: Zn/Ni-ZIF-8-800 carbon material and poly(caffeic acid) modified glassy carbon electrode **Arg-G/GC**: Arginine immobilized graphene modified glassy carbon electrode; **ERG/GCE**: electrochemically reduced graphene modified glassy carbon electrode; **SEP/MWCNTs/pPGE**: Nanosepiolite clay and multiwall carbon nanotubes modified electrochemically pre-treated pencil graphite electrode; **BiO-SPEs**: Bismuth oxide nanorod modified screen printed electrodes **AuNPs@TC8A/GN/GCE**: AuNPs modified by thiolated calix[8]arene anchored on graphene nanosheets/glassy carbon electrode; **MIP/ pABSA/GCE**: Molecular imprinted polymer film on poly(p-aminobenzene sulfonicacid) modified glassy carbon electrode; **MIP/PB/GCE:** Prussian blue and molecular imprinted polymer film modified glassy carbon electrode; MMIP/MCPE: Magnetic molecularly imprinted polymer-modified magnetic carbon paste; **BDDE**: boron-doped diamond; **B:CNWE**: boron-doped carbon nanowalls; **BSPCE** : Bare screen printed carbon electrode; **CPE:** Carbon paste electrode; **GCE**: Glassy carbon electrode; **DPV:** Differential pulse voltammetry; **LSV:** Linear sweep voltammetry

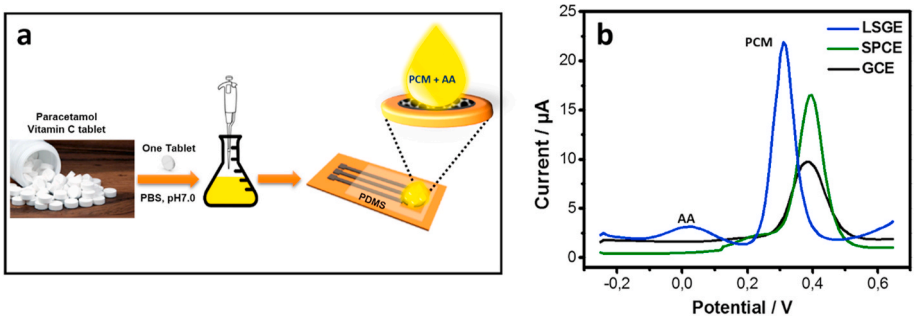

Fig. 5. (a) Schematic illustration of the pharmaceutical tablet sample preparation. **(b)** Simultaneous detection of AA and PCM by SWVs in a pharmaceutical tablet dissolved in 0.1 M PBS and 0.1M KCl (pH 7.0) at a GCE, SPCE, and LSGE.

evaluate the selectivity of the LSGE compared to the SPCE and the GCE. A summary of the results obtained in terms of peak-to-peak separation between PCM and AA peaks ($\Delta E_{AA\text{-}PCM}$) at SPCE, GCE, and LSGE was shown in Table 4S The results obtained showed that LSGE presented a higher $\Delta E_{AA\text{-}PCM}$, 280 mV between AA and PCM compared to 177 mV and 217 mV obtained at SPCE and GCE, respectively. Moreover, this high $\Delta E_{AA\text{-}PCM}$ can be attributed to the high electrocatalytic effect leading to potential peak shift of AA towards the negative potential values. Thus, the LSGE allows the sensitive and simultaneous detection of both analytes at a high-resolution (Fig. 5). However, the electrochemical response of AA on the SPCE was small and remarkably very close to that of PCM, indicating that the interference effect of AA with

PCM prevents the use of SPCE in real samples containing both analytes. Regarding the GCE, in addition to the problem of peak overlap that has been noticed, a small response towards these two molecules was measured.

Fig. 5S shows separated voltammograms of AA and PCM recorded at the SPCE, GCE, and LSGE at a scale in which all peaks can be distinguished. The LSGE demonstrated the ability to discriminate the possible interfering of AA on PCM without affecting the sensitivity of the sensor. Therefore, the LSGE can be considered an excellent choice and a promising sensor for selectively detection of pharmaceutical compounds.

4. Conclusion

In summary, a comparison study of the electrochemical performance of the LSGE as a new platform for electrochemical biosensors and the conventional SPCE in the detection of most common phenolic compounds and catecholamines compounds was performed for the first time. This study is of great interest since it presents the advantages of the use of a LSGE as a sensing platform for these compounds, results that could be extended to the development of novel highly sensitive and selective sensors. The excellent results obtained on the LSGE for PCM in terms of sensitivity (1.049 ± 0.176 μA μM^{-1}), LOD (31 nM), and electrocatalytic detection would make the LSGE a promising and excellent sensor platform for the routine, interference-free, and real-time analysis of PCM in pharmaceutical formulations. The LSGE sensing platform demonstrated the ability to be an alternative for the commercially available printed sensors, opening the window for the development of novel electrochemical sensors and biosensors. Despite the excellent features of LSG, the soft nature of the graphene material may lead to less durability as well as the decrease in conductivity due to the scratching of the surface. Hence, the doping of the LSG platform with highly conductive nanomaterials as well as optimizing the design of LSGs could enhance their mechanical stability. Furthermore, the LSGE would be a suitable candidate for integration into wearable and miniaturized electrochemical devices, providing real-time, sensitive, and selective detection of catecholamines in clinical diagnosis field, including identifying biomarkers for diseases such as biomarkers Alzheimer and Parkinson.

CRediT authorship contribution statement

Abdelghani Ghanam: Investigation, Methodology, Writing, Validation. **Abdellatif Ait Lahcen:** Writing - review & editing, Writing - original draft, Writing, Methodology, Validation, Investigation. **Tutku Beduk:** Writing - review & editing, Writing - original draft, Investigation, Methodology, Validation, Writing. **Husam N. Alshareef:** Investigation, Validation, Methodology, Writing - review & editing. **Aziz Amine:** Conceptualization, Supervision, Investigation, Writing - review & editing. **Khaled Nabil Salama:** Conceptualization, Supervision, Investigation, Writing - review & editing.

Declaration of competing interest

The authors declare that they have no known competing financial interests or personal relationships that could have appeared to influence the work reported in this paper.

Acknowledgments

The authors would like to express their acknowledgements to the financial support of funding from King Abdullah University of Science and Technology (KAUST), Saudi Arabia. Also, we thank the KAUST Sensor Initiative and KAUST Visiting Student Program for supporting this work. In addition, we would like to thank Dr Sakandar Rauf, Dr Veerappan Mani, Dr Sandeep G. Surya and Saravanan Yuvaraja for their suggestions and comments.

Appendix A. Supplementary data

Supplementary data to this article can be found online at https://doi.org/10.1016/j.bios.2020.112509.

References

Adebo, O.A., Medina-Meza, I.G., 2020. Molecules 25 (4).
Adhikari, B.R., Govindhan, M., Chen, A.C., 2015. Electrochim. Acta 162, 198–204.
Ahmad, R., Wolfbeis, O.S., Hahn, Y.B., Alshareef, H.N., Torsi, L., Salama, K.N., 2018. Mater Today Commun 17, 289–321.
Amine, A.M.H., 2019. In: Encyclopedia of Analytical Science, third ed. ed. Elsevier, pp. 85–98.
Anithaa, A.C., Asokan, K., Sekar, C., 2017. Electrochim. Acta 237, 44–53.
Attar, A., Cubillana-Aguilera, L., Naranjo-Rodriguez, I., de Cisneros, J.L.H.H., Palacios-Santander, J.M., Amine, A., 2015. Bioelectrochemistry 101, 84–91.
Azzouz, A., Goud, K.Y., Raza, N., Ballesteros, E., Lee, S.E., Hong, J., Deep, A., Kim, K.H., 2019. Trac-Trend Anal Chem 110, 15–34.
Bayraktepe, D.E., Yazan, Z., 2020. Electroanal 32 (6), 1263–1272.
Bayraktepe, D.E., Yazan, Z., Onal, M., 2019. Talanta 203, 131–139.
Beduk, T., Lahcen, A.A., Tashkandi, N., Salama, K.N., 2020. Sensor. Actuator. B Chem. 128026.
Biswas, S., Naskar, H., Pradhan, S., Wang, Y., Bandyopadhyay, R., Pramanik, P., 2020. Talanta 206.
Cardoso, A.R., Marques, A.C., Santos, L., Carvalho, A.F., Costa, F.M., Martins, R., Sales, M.G.F., Fortunato, E., 2019. Biosens. Bioelectron. 124, 167–175.
Chen, Y., Xu, J.H., Yang, Y.J., Zhao, Y.T., Yang, W.Y., He, X., Li, S.B., Jia, C.Y., 2016. J Mater Sci-Mater El 27 (3), 2564–2573.
Dai, Y.L., Li, X.Y., Lu, X.J., Kan, X.W., 2016. Microchim Acta 183 (10), 2771–2778.
de Holanda, L.F., Ribeiro, F.W.P., Sousa, C.P., Casciano, P.N.D., de Lima-Neto, P., Correia, A.N., 2016. J. Electroanal. Chem. 772, 9–16.
de Moraes, E.E., Tonel, M.Z., Fagan, S.B., Barbosa, M.C.D., 2019. J. Mol. Model. 25, 302, 302.
Della Pelle, F., Gonzalez, M.C., Sergi, M., Del Carlo, M., Compagnone, D., Escarpa, A., 2015. Anal. Chem. 87 (13), 6905–6911.
Engin, C., Yilmaz, S., Saglikoglu, G., Yagmur, S., Sadikoglu, M., 2015. Int J Electrochem Sc 10 (2), 1916–1926.
Fenzl, C., Nayak, P., Hirsch, T., Wolfbeis, O.S., Alshareef, H.N., Baeumner, A.J., 2017. ACS Sens. 2 (5), 616–620.
Ghanam, A., Lahcen, A.A., Amine, A., 2017. J. Electroanal. Chem. 789, 58–66.
Griffiths, K., Dale, C., Hedley, J., Kowal, M.D., Kaner, R.B., Keegan, N., 2014. Nanoscale 6 (22), 13613–13622.
Guzman-Hernandez, D.S., Martinez-Cruz, M.A., Ramirez-Silva, M.T., Romero-Romo, M., Corona-Avendano, S., Mendoza-Huizar, L.H., Palomar-Pardave, M., 2016. Anal Methods-Uk 8 (44), 7868–7872.
Hawley, M.D., 1967. Journal of American Chemcial Society 89.
Hwang, J.Y., El-Kady, M.F., Wang, Y., Wang, L.S., Shao, Y.L., Marsh, K., Ko, J.M., Kaner, R.B., 2015. Nano Energy 18, 57–70.
Ibanez-Redin, G., Wilson, D., Goncalves, D., Oliveira, O.N., 2018. J. Colloid Interface Sci. 515, 101–108.
Jesus, F., Goncalves, A.C., Alves, G., Silva, L.R., 2019. Food Res. Int. 116, 600–610.
Ji, D.Z., Xu, N., Liu, Z.X., Shi, Z.Y.J., Low, S.S., Liu, J.J., Cheng, C., Zhu, J.W., Zhang, T. K., Xu, H.X., Yu, X.J., Liu, Q.J., 2019. Biosens. Bioelectron. 129, 216–223.
Karikalan, N., Karthik, R., Chen, S.M., Velmurugan, M., Karuppiah, C., 2016. J. Colloid Interface Sci. 483, 109–117.
Kenarkob, M., Pourghobadi, Z., 2019. Microchem. J. 146, 1019–1025.
Kumar, S., Lei, Y.J., Alshareef, N.H., Quevedo-Lopez, M.A., Salama, K.N., 2018. Biosens. Bioelectron. 121, 243–249.
Kurra, N., Jiang, Q., Nayak, P., Alshareef, H.N., 2019. Nano Today 24, 81–102.
Lahcen, A.A., Amine, A., 2018. Anal. Lett. 51 (3), 424–441.
Lee, S.H., Kim, K.Y., Yoon, J.R., 2020. NPG Asia Mater. 12 (1).
Li, J.H., Liu, J.L., Tan, G.R., Jiang, J.B., Peng, S.J., Deng, M., Qian, D., Feng, Y.L., Liu, Y. C., 2014. Biosens. Bioelectron. 54, 468–475.
Lin, J., Peng, Z.W., Liu, Y.Y., Ruiz-Zepeda, F., Ye, R.Q., Samuel, E.L.G., Yacaman, M.J., Yakobson, B.I., Tour, J.M., 2014. Nat. Commun. 5.
Liu, W.J., Shi, Q.F., Zheng, G., Zhou, J., Chen, M., 2019. Anal. Chim. Acta 1075, 81–90.
Lu, W.H., Ming, W.N., Zhang, X.S., Chen, L.X., 2016. Electrophoresis 37 (19), 2487–2495.
Mahmoud, B.G., Khairy, M., Rashwan, F.A., Banks, C.E., 2017. Anal. Chem. 89 (3), 2170–2178.
Nadifiyine, S., Haddam, M., Mandli, J., Chadel, S., Blanchard, C.C., Marty, J.L., Amine, A., 2013. Anal. Lett. 46 (17), 2705–2726.
Nayak, P., Kurra, N., Xia, C., Alshareef, H.N., 2016. Adv Electron Mater 2 (10).
Niedzialkowski, P., Cebula, Z., Malinowska, N., Bialobrzeska, W., Sobaszek, M., Ficek, M., Bogdanowicz, R., Anand, J.S., Ossowski, T., 2019. Biosens. Bioelectron. 126, 308–314.
Palanisamy, S., Ramaraj, S.K., Chen, S.M., Yang, T.C.K., Yi-Fan, P., Chen, T.W., Velusamy, V., Selvam, S., 2017. Sci Rep-Uk, vol. 7.
Ramirez, C., del Valle, M.A., Isaacs, M., Armijo, F., 2016. Electrochim. Acta 199, 227–233.
Ramlan, A.H., Sirat, S., Ismail, E., Buys, Y.F., Purwanto, H., Mustafah, Y., Din, M.F.M., Ani, M.H., 2019. Mater Today-Proc 7, 675–685.
Sanghavi, B.J., Mobin, S.M., Mathur, P., Lahiri, G.K., Srivastava, A.K., 2013. Biosens. Bioelectron. 39 (1), 124–132.

Scalbert, A., Manach, C., Morand, C., Remesy, C., Jimenez, L., 2005. Crit Rev Food Sci 45 (4), 287–306.
Schindler, S., Bechtold, T., 2019. J. Electroanal. Chem. 836, 94–101.
Schindler, S.B.T., 2019. Mechanistic Insights into the Electrochemical Oxidation of Dopamine by Cyclic Voltammetr.
Sharp, M., Petersson, M., Edstrom, K., 1979. J. Electroanal. Chem. 95 (1), 123–130.
Su, C.L., Li, Z.Y., Zhang, D., Wang, Z.M., Zhou, X., Liao, L.F., Xiao, X.L., 2020. Biosens. Bioelectron. 148.
Talarico, D., Arduini, F., Constantino, A., Del Carlo, M., Compagnone, D., Moscone, D., Palleschi, G., 2015. Electrochem. Commun. 60, 78–82.
Taleb, M., Ivanov, R., Bereznev, S., Kazemi, S.H., Hussainova, I., 2018. J. Electroanal. Chem. 823, 184–192.
Teng, Y., Fan, L.M., Dai, Y.L., Zhong, M., Lu, X.J., Kan, X.W., 2015. Electrochemical sensor for paracetamol recognition and detection based on catalytic and imprinted composite film. Biosens. Bioelectron. 71, 137–142.
Tohma, H., Gulcin, I., Bursal, E., Goren, A.C., Alwasel, S.H., Koksal, E., 2017. J Food Meas Charact 11 (2), 556–566.
Tyszczuk-Rotko, K., Beczkowska, I., Wojciak-Kosior, M., Sowa, I., 2014. Talanta 129, 384–391.
Tyszczuk-Rotko, K., Jaworska, I., Jedruchniewicz, K., 2019. Microchem. J. 146, 664–672.
Viacava, G.E., Roura, S.I., Lopez-Marquez, D.M., Berrueta, L.A., Gallo, B., Alonso-Salces, R.M., 2018. Food Chem. 260, 239–273.
Vinson, J.A., 2019. J Agr Food Chem 67 (14), 3865–3870.
Wee, Y., Park, S., Kwon, Y.H., Ju, Y., Yeon, K.M., Kim, J., 2019. Biosens. Bioelectron. 132, 279–285.
Wierzbicka, E., Sulka, G.D., 2016. J. Electroanal. Chem. 762, 43–50.
Wong, A., Santos, A.M., Fatibello, O., 2018. Sensor. Actuator. B Chem. 255, 2264–2273.
Xu, G.Y., Jarjes, Z.A., Wang, H.W., Phillips, A.R.J., Kilmartin, P.A., Travas-Sejdic, J., 2018a. Acs Appl Mater Inter 10 (49), 42136–42145.
Xu, G.Y., Jarjesa, Z.A., Desprez, V., Kilmartin, P.A., Travas-Sejdic, J., 2018b. Biosens. Bioelectron. 107, 184–191.
Xu, Z., Zhang, M.Q., Zou, H.Q., Liu, J.S., Wang, D.Z., Wang, J., Wang, L.D., 2019. J. Electroanal. Chem. 841, 129–134.
Xuan, X., Kim, J.Y., Hui, X., Das, P.S., Yoon, H.S., Park, J.Y., 2018. Biosens. Bioelectron. 120, 160–167.
Ye, R.Q., James, D.K., Tour, J.M., 2018. Laser-induced graphene. Accounts Chem. Res. 51 (7), 1609–1620.
You, R., Liu, Y.Q., Hao, Y.L., Han, D.D., Zhang, Y.L., You, Z., 2019. Adv Mater.
Zhang, C., Xie, Y.C., Zhang, C., Lin, J., 2019a. Carbon 153, 585–591.
Zhang, F., Alhajji, E., Lei, Y.J., Kurra, N., Alshareef, H.N., 2018a. Adv Energy Mater. 8 (23).
Zhang, W.Q., Zong, L.K., Liu, S.Q., Pei, S., Zhang, Y.S., Ding, X.M., Jiang, B., Zhang, Y.P., 2019b. Biosens. Bioelectron. 131, 200–206.
Zhang, Y., Chen, X.Y., 2019. Nanoscale 11 (41), 19105–19118.
Zhang, Y., Huang, Z.Y., Wang, L.T., Wang, C.M., Zhang, C.D., Wiese, T., Wang, G.D., Riley, K., Wang, Z., 2018b. Anal. Chem. 90 (7), 4733–4740.
Zhang, Y., Jiang, X.T., Zhang, J.J., Zhang, H., Li, Y.C., 2019c. Biosens. Bioelectron. 130, 315–321.